iVES OENO One vine & wine

DOI: https://doi.org/10.20870/oeno-one.2024.58.4.8209

OPEN ACCESS

15TH INTERNATIONAL TERROIR CONGRESS MENDOZA, ARGENTINA

ORIGINAL RESEARCH ARTICLE

Water status assessment in grapevines using plant electrophysiology

Amanda Malvessi Cattani[1,a], Léo de Riedmatten[2,a], Julien Roulet[2], Tara Smit-Sadki[1], Esteban Alfonso[1], Andrzej Kurenda[2], Eric Remolif[3], Moritz Graeff[2], Markus Rienth[1,*]

[1] University of Sciences and Art Western Switzerland, Changins College for Viticulture and Enology, Nyon, Switzerland.
[2] Vivent SA, Gland, Switzerland.
[3] Agroscope, Nyon Switzerland.

[a] The authors contributed equally to this work.

This article is published in cooperation with the XVth International Terroir Congress, 18-22 November 2024, Mendoza, Argentina.

Guest editors: Federico Berli, Jorge Prieto and Martín Fanzone.

ABSTRACT

Traditional methods for assessing vine water status, such as the Scholander pressure chamber, are time-consuming, punctual and labour-intensive. The development of alternative methods which are accurate, reliable and can provide real-time information on vine water status is a necessity for farmers all over the world. This study proposes the use of plant electrophysiology as a novel approach for real-time water status assessment in grapevines. We conducted four climate chamber experiments with potted grapevines under different irrigation regimes. Various morphological and physiological assessments were performed in parallel with electrophysiological measurements to correlate classic water status assessment methods with plant electrophysiological signals. Two machine learning approaches based on classification and regression were employed to train the prediction models. Results obtained from both models indicate significant differences in irrigation status between well-watered and water-deficit plants, with the latter showing reduced growth and physiological activity, confirming the water stress status of the plant. While the binary classification model successfully differentiates between well-watered and water-deficit plants, its practical use is limited. Therefore, a regression model was developed to directly predict predawn leaf water potential. To the best of our knowledge, this is the first time that electrical signals are correlated with vine water potential measurements. The findings presented here thus provide a promising new tool for future real-time and remote monitoring of vine water status to manage irrigation and adapt agronomic strategies. Nevertheless, validation and optimisation of the models are still necessary, particularly under field conditions.

KEYWORDS: Terroir 2024, grapevines, drought, electrophysiology, plant electrical signals

*correspondence:
markus.rienth@changins.ch

Associate editor:
Jorge Prieto

Received:
21 June 2024

Accepted:
3 October 2024

Published:
4 November 2024

This article is published under the **Creative Commons licence** (CC BY 4.0).

Use of all or part of the content of this article must mention the authors, the year of publication, the title, the name of the journal, the volume, the pages and the DOI in compliance with the information given above.

INTRODUCTION

The ramifications of climate change on viticulture encompass profound alterations in berry metabolism precipitated by elevated temperatures and primarily drought-induced water stress (Charrier *et al*., 2018; Scholasch and Rienth, 2019; van Leeuwen *et al*., 2024). As global temperatures continue to rise, the seasonal water balance of vineyards is becoming more and more negative. Higher evapotranspiration rates, coupled with reduced rainfall during the growing season, pose significant challenges to current viticulture practices (Rienth and Scholasch, 2019; van Leeuwen *et al*., 2019). Grapevine development is significantly influenced by severe water deprivation, which alters leaf and root biomass allocation. While light to moderate water deficits can enhance berry quality and thus improve the quality of the wine, severe water stress can cause substantial yield losses and disrupt berry ripening. Water deficit stress leads to higher sugar concentration, resulting in elevated alcohol levels, reduced acidity due to accelerated malic acid degradation, and general changes in aroma compounds, ultimately compromising wine typicity (Pons *et al*., 2017; Rienth *et al*., 2014; Rienth *et al*., 2021; Scholasch and Rienth, 2019; van Leeuwen *et al*., 2019). Hence, monitoring the water status of vines is an essential step in viticulture practices to ensure the harvesting of high-quality fruits suitable for all subsequent uses. Commonly, the water status of grapevines is assessed using destructive batch measurements such as the Scholander pressure chamber (Scholander *et al*., 1965), which, while providing accurate punctual information about plant water status, is both time- and labour-intensive (Rienth and Scholasch, 2019). An alternative method involves using sap-flow sensors, increasingly employed for irrigation management due to their capability of obtaining real-time data. However, the high cost and energy demand of existing sap-flow sensors limit their applicability for large-scale plant health monitoring (Rienth and Scholasch, 2019). This underscores the need for new, non-destructive tools that can provide real-time and precise data on vine water status to manage irrigation and/or adjust agronomic strategies.

To survive variations in water availability, plants have developed a diverse set of fine-tuned mechanisms, which include stomatal and photosynthesis regulation, changes in phytohormone balance, and leaf osmotic adjustments (Gambetta *et al*., 2020). Many of these stress-related processes may be linked with changes in the electrical properties of plant tissue at different levels of organisation (Zhang *et al*., 2020; Xing *et al*., 2019). Extracellular electrophysiology in the configuration used in this study is sensing spatiotemporal changes in charged molecules distribution between electrodes *i.e*. across the plant stem. Charge carriers, such as inorganic ions taken from the soil, or organic molecules dissociated in the aqueous environment of the cells, are subject to active (transport with the use of energy) and passive (flow of water to the cells or the air from extracellular spaces) concentration changes, when the water status of the plant is varying. An example of this complex process can be the regulation of stomata opening (Roelfsema *et al*., 2004). Open stomata enable evapotranspiration and induce uptake and transport of water from the soil to the leaves. Water availability in the root area results in a stable transpiration stream and a relatively low water potential gradient between the soil and the stem (Feng *et al*., 2016). During limited water availability, the water potential gradient between the soil and stem increases, leading to gradual changes in the extracellular environment (Feng *et al*., 2016). This will cause an adjustment to the transmembrane potential of the cells which will be detected by electrodes as electrical potential variations. Other processes potentially linked with electrophysiological responses to drought stress may not be directly related to the ion concentration changes but to phenomena affecting overall plant physiology or morphology. Cavitation originating from turbulent water flow in the xylem vessels can cause vibrations (Vilagrosa *et al*., 2012), mechanically affecting contact between electrodes and plant cells and inducing fast changes in electrical potential. Finally, drought stress may change cell excitability and facilitate the induction of fast and long-distance electrical signals, studied usually in the context of wound-induced or biotic stress (Fromm and Lautner, 2007; Kurenda *et al*., 2024).

Although cell electrophysiology has been explored for a long time (Fromm and Lautner, 2007), the recent progress in hardware and software technologies (Tran *et al*., 2019) has opened the possibility of fast advances in understanding the basic processes and practical applications of plant electrical potential variations. The hardware and software developments enabled higher signal-to-noise ratio recordings, efficient collection and transfer of large datasets, and the application of machine learning (ML) techniques for more effective interpretation of recorded signals. Among the aforementioned achievements, the most significant technological advancement enabling fast and precise analysis of big datasets, such as plant electrophysiological recordings, is ML. This analytical method, when applied in agronomical systems, offers farmers greater autonomy and enhances the sustainability of agricultural systems (Araújo *et al*., 2023). ML is a process where algorithms learn patterns from input data to make predictions or decisions, producing outputs without explicit programming for specific tasks. To this end, the first critical step is to gather and prepare the data that will serve as input to the ML models. Robust and well-designed trials are fundamental for the creation of successful models. Once the data has been gathered, it is divided into training and test sets. The training set is used to train the model, while the test set is used to evaluate its performance.

The Swiss-based deep tech company Vivent Biosignals (Gland, Switzerland) designed biosensors which can record and process electrophysiological data across a wide range of plant species (Tran *et al*., 2019). In avocado trees, short-term variations in plant electrical potential were strongly associated with drought stress intensity (Gil and Vargas, 2023). For tomatoes, the use of electrophysiological signals has been described as an innovative approach for real-time stressors identification (drought, nutrient deficit and spider mite infection) with 80 % accuracy (Najdenovska *et al*., 2021).

Recently, the electrophysiology of grapevines has started to be explored, however, no works regarding the correlation with drought stress have been published yet. With the help of specialised electrodes, amplifiers coupled with a data recorder and the development of ML models, we introduce in this work a pioneering strategy for water status assessment in grapevines. To build datasets for the ML models, different series of water stress experiments were conducted. Based on classical measurements of various ecophysiological parameters and electrical potential recordings, accurate models were developed and validated using test sets, providing alternative solutions for a more dynamic and smart viticulture farming.

MATERIALS AND METHODS

1. Drought assays experimental design

To generate a dataset from plants experiencing different states of water deficit, four series of climate chamber experiments (16 plants each), were conducted on cuttings of *Vitis vinifera* L. cv Cabernet-Sauvignon under different irrigation regimes. The vines used in this work were propagated through hardwood cuttings, which were produced in the previous winter season and maintained at 5 °C. For vegetative growth, plants were placed in pots of 1 L (13 cm diameter) containing a peat-rich substrate mix (55 % blonde peat, 10 % compost, 10 % coconut fibre, 15 % topsoil and 10 % perlite). After 14-16 weeks of vegetative growth in the greenhouse (20 °C day/18 °C night, 50-60 % humidity with supplemental lighting from September to May: 100 W/m² for 12 hours daily), the vines were transferred to 0.6 m² × 1.2 m height growing area climate chambers (Polyklima, Germany). They were grown under 25 °C day/15 °C night; 14/10 lighting hours and 55 % of humidity. In total, 2 groups of 8 plants each were submitted to two different irrigation regimes: well-watered (WW), where watering was kept around 80-100 % of field capacity (FC) and water-deficit (WD) where irrigation levels were managed depending on the trial experimental design. In total, 2 weeks of severe water stress were performed on trials 1 and 2 (Figure 1A). The irrigation of WD treatment was cessed after two days of plant adaptation in the climate chambers. In trial 3, WD plants were 5 days chamber-acclimated (same

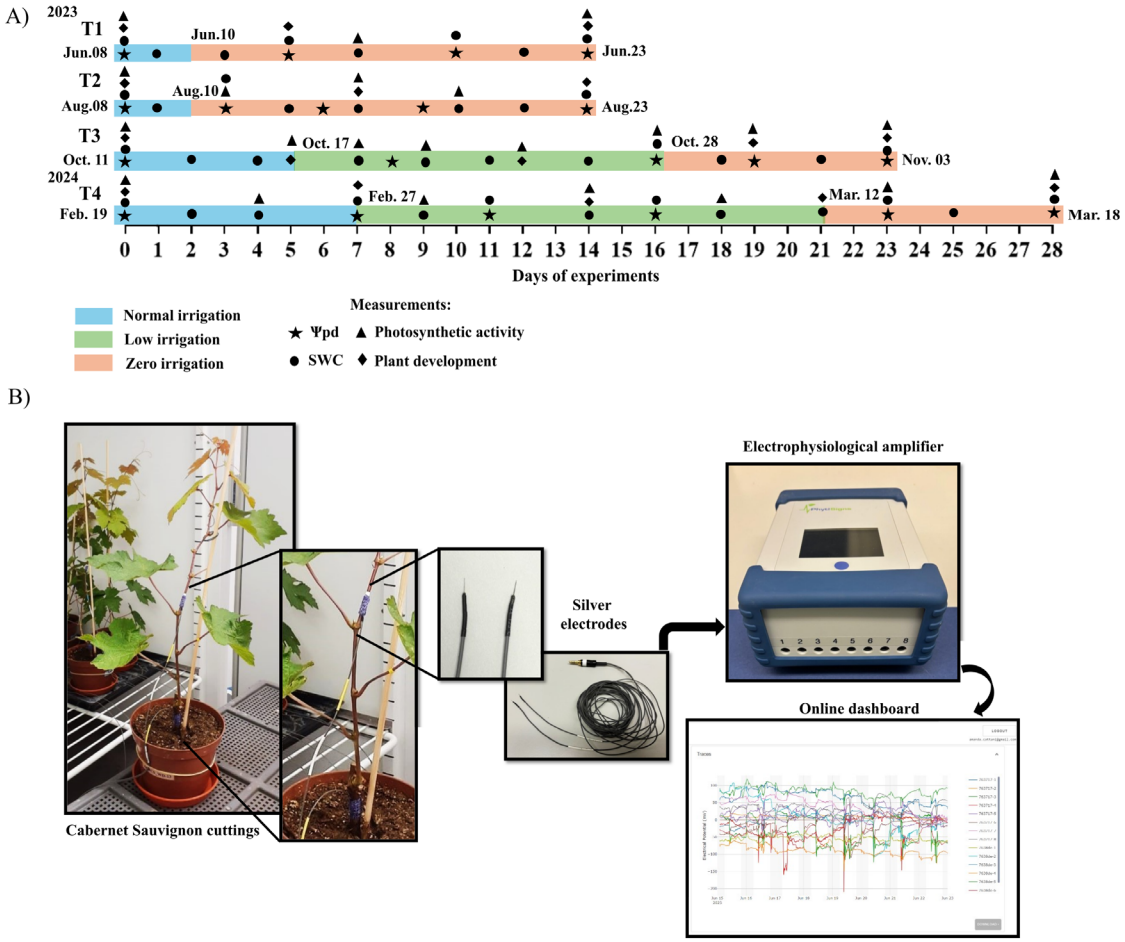


FIGURE 1. Timeline and experimental design of grapevine drought trials.

(A) Schematic overview of the irrigation regimes (normal, low and zero) applied during trials 1-4. The timeline indicates the start and end dates of each trial, highlighting the implementation date of the new irrigation regime. The frequency of key ecophysiological measurements is also depicted. SWC: soil water content; Ψpd: predawn leaf water potential. (B) Experimental setup for *Vitis vinifera* cv. Cabernet-Sauvignon cuttings, showing the attachment of two silver electrodes: one on the plant trunk (reference electrode) and another on the middle of the vegetative stem (active electrode). The electrodes were connected to a Vivent electrophysiological amplifier, with signal quality continuously monitored *via* Vivent online dashboard.

irrigation as WW) followed by 10 days of low irrigation (approximately 50 % FC) and 7 days of non-irrigation (Figure 1A). Trial 4 was performed for a total of 4 weeks, with 1 week of acclimatisation, 2 weeks of low irrigation (as trial 3) and 1 week of non-irrigation (Figure 1A). Soil water content (SWC) was monitored 3 times per week by pot weighing (Figure 1A). The SWC was converted to % FC based on the specific SWC determined for the potting mix at 100 % FC.

2. Morphological and physiological plant monitoring in response to stress

Predawn leaf water potential (Ψpd) was assessed on fully developed adult leaves from all WW and WD plants using a Scholander pressure chamber (Scholander *et al*., 1965; PMS Instrument, USA). Ψpd measurements were performed every 3-7 days, depending on the trial and the irrigation regime (Figure 1A). Morphological traits, such as stem length, number of nodes and stem diameter were monitored every 5-7 days to follow plant-by-plant development (Figure 1A). Photosynthetic activity *via* stomatal conductance (gs), net photosynthesis (A), transpiration (E), photosynthetic water use efficiency (WUE), leaf-to-air vapour-pressure deficit (VPD) and sub-stomatal CO_2 concentration (Ci) was measured in all plants at least two times per week using a portable photosynthesis system (CIRAS-3, PP systems, USA; Figure 1A). At the end of each trial, total biomass and plant water content were estimated considering fresh and dry mass for each plant organ. The dry mass was obtained by oven-drying the fresh mass at 65 °C for 48 h.

3. Plant electrophysiology measurements and data preprocessing.

In each trial, 16 plants were divided randomly into two equally numerous groups and placed in climate chambers. Electrophysiology measurements were performed with PSR8 Vivent biosensor which features an 8-channel electrophysiology amplifier with high input impedance of 200 MOhm. The measurement circuit for each plant included 3-meter coaxial cables and two silver-plated needle electrodes: one inserted into the plant trunk as a reference electrode, and the other into the middle of the vegetative stem as the active electrode (Figure 1B). The electrical potential difference was continuously recorded throughout the trial at a sampling rate of 256 Hz. Before analogue-to-digital conversion, the signal underwent analogue notch filtering to eliminate 50 and 100 Hz mains noise. The recorded signals were stored in the internal memory of the PSR8 device while being simultaneously transmitted to a server for real-time re-sampling, display, and analysis *via* the Vivent online dashboard. For the developments of ML models, the signals recorded at 256 Hz were down-sampled to 1 Hz.

4. Dataset preparation and model training using electrophysiological signals

The dataset consists of univariate time series representing the electrical potential recording of each plant during each trial (Figure 2A). We segmented the data into consecutive rolling windows, each covering 24 hours. These windows were created to overlap, with a 6-hour shift between each successive window (Figure 2B). Segmenting time series into shorter windows is common practice in training ML models (Fawaz *et al*., 2018). This is done for several reasons, including reducing complexity, as long time series can be too large and complex to process directly, as well as focusing on local structures since time series often have varying structures at different time scales (*e.g*., daily *vs*. weekly patterns). Subsequently, we applied a Debauchies 2 discrete wavelet decomposition to each window, yielding wavelet coefficients at 14 different levels of decomposition (Mallat, 1989; Figure 2C).

The choice of decomposing the raw signals into their wavelet coefficients is motivated by its ability to capture features at different frequency and time scales, reduce noise, and handle non-stationarity effectively, enabling us to obtain rich and localised time-frequency representations of the data (Amin *et al*., 2015; Wang *et al*., 2018). From each wavelet coefficient, we extracted a comprehensive set of features to capture relevant information. This included standard statistical measures such as minimum, maximum, and mean, computed for each level of decomposition. Additionally, Catch22 features (Lubba *et al*., 2019), a curated set of features designed for time series analysis, were used (Figure 2D). From there, we gather all features extracted from each wavelet coefficient to end up with a matrix of dimensions $W \times F$, where W is the number of wavelet coefficients and F is the number of extracted features. This matrix is flattened into a one-dimensional (1D) feature vector and represents a sample that is fed as input into our models. Therefore, the resulting dataset used for training and testing our models is a collection of 1D feature vectors, with each vector being a representation of a 24-hour window of raw data from a single plant collected by Vivent sensors.

The dataset was divided into a training set and two test sets. The training set was used to train the model, while the test sets were utilised post-training to impartially evaluate its performance. The first test set, T123, consisted of a subset of plants randomly selected from the first three experiments. This dataset was split by plant to prevent any information leakage (Kaufman *et al*., 2012), thereby safeguarding against bias at the biological replicate level and ensuring robustness in our analysis. The second test set, T4, was used to assess the trained model's performance on data from all the plants in the fourth experiment, which were entirely unseen during training. This is done to test the model's generalisation capabilities to new experiments unseen during training, as each experiment occurs in different conditions and results in unique signatures in the signals. Using separate trials in training as well as testing ensures the model does not learn to use experiment-specific noise in its decision-making. In summary, data from the first three experiments were used for the training set and the first test set (T123), while data from the fourth experiment was kept separate from the second test set (T4).

For hyperparameter optimisation, which was only performed on the training set, we employed a leave-one-group-out strategy, with each group corresponding to one of the first three experiments. This means that for each set of

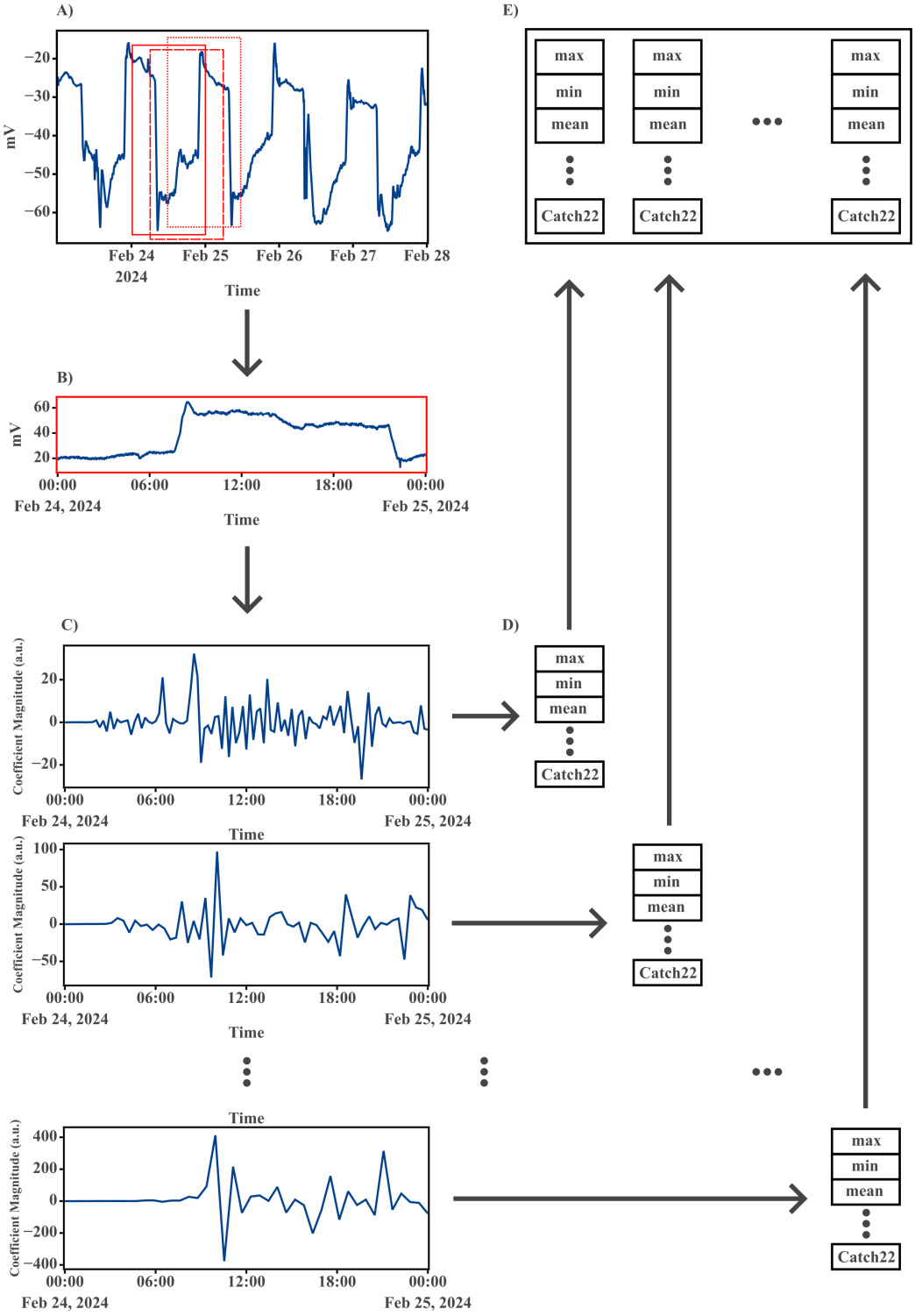


FIGURE 2. Data processing pipeline for model development.

(A) Example of an electrophysiology signal recorded by Vivent biosensors over 5 days. The diurnal pattern is induced by day/night light intensity changes. The red rectangles represent the segmentation process resulting in 3 windows of 24-hour length with 6-hour shifts between them. (B) Magnification of signal in a 24-hour window from the red solid-line rectangle in (A). (C) Result of the Debauchies 2 wavelet decomposition of a 24-hour long signal into 14 time-series covering different frequency bands of the original raw signal. (D) For each of the resulting wavelet coefficients, features such as minimum, maximum and mean, as well as a set of features from the Catch22 library were extracted. (E) Finally, all these features were concatenated into one matrix of dimensions W × F, where W is the number of wavelet coefficients and F is the number of extracted features. Before being fed as input to the models, the matrix was flattened into a one-dimensional feature vector.

hyperparameters attempted during the optimisation process, the model is trained on two experiments and tested on the left-out experiment, leading to three iterations (one for each pair of experiments). This enables a more robust and accurate estimate of the model performance. We used the Bayesian optimisation Python library Optuna (Akiba *et al.*, 2019) to identify the most suitable hyperparameters for our models.

For the training phase, two different methodologies were used: 1) classification, where the model outputs the probability of a feature vector being in a WD state and 2) regression, where the model predicts the Ψpd value of a feature vector. Since both these strategies are 'supervised' learning approaches, they require labels in the training phase of the models, meaning each feature vector must be paired with the correct 'class' or target value to guide the learning process (Goodfellow *et al.*, 2016). Since the classification model predicts the probability of a feature vector being in a WD state, a binary labelling system was used. The group of plants that undergo an irrigation restriction phase are labelled as WW (probability of being in WD is 0) before the restriction phase begins and as WD (probability of being in WD is 1) afterwards. Here, we underscore the importance of including a control group of vines to prevent the model from mistakenly learning features related to plant growth or development as indicators of water deficiency. For the regression strategy, the model aims to predict the actual Ψpd based on the feature vector, therefore, the data were labelled with the Ψpd measurements that were made during the experiments. Since the Ψpd was only measured periodically in comparison to our rolling 24-hour windows with a 6-hour shift, we linearly interpolated between the missing values to have a continuous annotation for Ψpd for each feature vector.

In both these modelling strategies, the feature vectors were used as input to an eXtreme gradient-boosted (XGB) tree algorithm (Chen and Guestrin, 2016). We chose XGB as it is widely used for solving classification and regression problems in ML due to its performance, flexibility and interpretability, amongst other advantages. XGB makes use of decision trees, another popular ML algorithm which works by iteratively splitting data into branches based on feature values to make predictions, resulting in a tree-like structure (Hastie *et al.*, 2009). In summary, XGB is chosen for classifying vine plants as being in a WW or WD state and for predicting the Ψpd value of a vine plant.

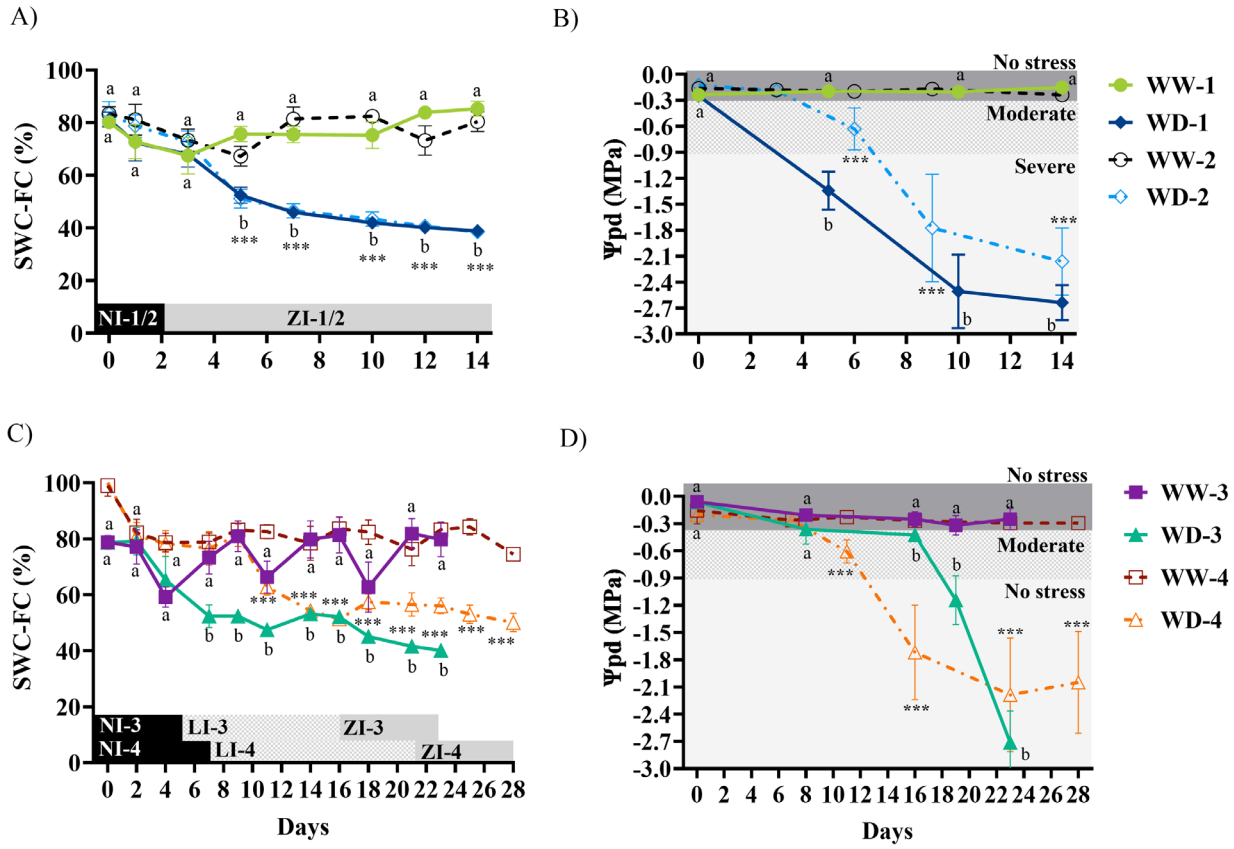


FIGURE 3. Conventional water status assessment of grapevines.

(A) The percentage of soil water content (SWC) in relation to field capacity (FC) was estimated *via* plant pot weighting every 2 days during all experiments of trials 1 and 2. (B) Predawn leaf water potential (Ψpd) was measured in all plants for trials 1 and 2 using a Scholander pressure chamber. (C) The percentage of SWC-FC for trials 3 and 4 was determined in the same way as mentioned for trials 1 and 2. Periods of normal (NI), low (LI) and zero irrigation (ZI) of trials 1-4 are delimited in the plots. WW: well-watered; WD: water-deficit; 1, 2, 3 or 4 indicates the trial number. The same letters represent a lack of statistically significant differences between treatments in the same trial for each time-point (trials 1 and 3). Asterisks were used for trials 2 and 4 (***—$p < 0.05$). Values are represented as mean ± SEM.

5. Statistical analysis

All statistical analyses were performed with GraphPad Prism version 10.0.0 for Windows, GraphPad Software, USA. Comparisons between WW and WD on each trial for each time point were analysed by Student's t-test ($p < 0.05$).

RESULTS AND DISCUSSION

1. Assessing water status of grapevines by conventional methods: from short-severe to long-moderate drought stress scenarios

To develop accurate models for drought prediction in grapevines based on electrophysiological signals, we conducted different series of drought experiments under controlled conditions in climate chambers using potted grapevines. This approach permitted us to minimise unquantifiable variation from other biotic and abiotic factors not related to water availability that could have affected plant electrical signals. The experiments were split into two series of short-severe (trials 1 and 2) and long-moderate water deficit stress (trials 3 and 4). All over the short-severe water deficit experiments, the irrigation of WW-1 and WW-2 plants was kept at 77.0 ± 6.9 and 77.8 ± 6.8 % FC, respectively (Figure 3A). After 5 days without watering, WD-1 and WD-2 plants reached 52.5 ± 3.1 and 51.1 ± 3.5 % FC, respectively and significant differences could be observed between treatments (Figure 3A). In agreement with SWC data, the water deficit status of WD-1 and WD-2 vines was confirmed by assessing the Ψpd. From day 7, WD-1 plants were already under severe drought stress (–1.3 ± 0.2 MPa). For WD-2, this point was reached three days after, with a Ψpd of –1.8 ± 0.2 MPa (Figure 3B).

After 14 days, grapevine development was severely affected (Figure S1) and SWC was at 38.5 ± 1.1 and 38.9 ± 1.9 % FC for WD-1 and WD-2 plants, respectively (Figure 3A). The measures of Ψpd confirmed that WD-1 and WD-2 grapevines were extremely affected by water deficit (–2.6 ± 0.2; –2.2 ± 0.4 MPa; Figure 3B). All over the experiment, Ψpd of WW-1 and WW-2 plants remained at around –0.19 ± 0.06 and –0.19 ± 0.04 MPa (Figure 3B), indicating no water deficit stress (van Leeuwen *et al*., 2009; Lovisolo *et al*., 2010.; Rienth and Scholasch, 2019).

In the long-moderate trials, irrigation of WD-3 was reduced by 50 % from day 5 and no more watering was performed from day 16. In an even longer approach, (trial 4) the reduction of irrigation by 50 % on WD-4 began after 1 week of plant acclimation (Figure 1A). From day 21 no more irrigation was performed. During the entire experiment, water availability was not limiting for control groups WW-3 and WW-4 and SWC values were maintained at 74.8 ± 9.5 and 82.1 ± 6.9 % FC (Figure 3C). Although a greater oscillation of SWC was observed within plants of the WW-3 group, the Ψpd was not affected and similar values for WW-3 and WW-4 (–0.22 ± 0.12 and –0.24 ± 0.18 MPa, respectively) were observed, confirming the non-stressed status of plants (van Leeuwen *et al*., 2009; Lovisolo *et al*., 2010; Rienth and Scholasch, 2019; Figure 3D). Regarding WD treatments, a significant decrease in SWC was observed from day 7 for WD-3 (52.4 ± 4.0 % FC) while only 4 days after, the SWC of WD-4 grapevines presented a reduction (62.8 ± 2.9 % FC) compared to well-watered plants (Figure 3C). The plant water status measured *via* Ψpd revealed WD-3 plants at a moderate water deficit stress on day 16 (–0.43 ± 0.05 MPa). For WD-4, a similar water deficit appeared four days before (–0.61 ± 0.13 MPa; Figure 3D). Severe water deficit stress scenario was also observed before for WD-4 (day 16: –1.72 ± 0.52 MPa; Figure 3D) compared to WD-3 vines (day 19: –1.14 ± 0.27 MPa). Plants from WD-4 were older and more numerous in nodes (day 0: 11.4 ± 2.3 nodes), with a higher leaf area (Figure S1) than WD-3 (day 0: 8.5 ± 1.7), which may explain the faster water loss observed on WD-4. The growth of WD-plants was strongly affected in both trials 3 and 4 (Figure S1). Even if the slope of the water deficit stress was less accentuated in the long-moderate assays, similar levels of Ψpd were found at the end of all trials (Figure 3), indicating a severe water stress deficit in all WD-tested plants, regardless of the drought stress approach.

The use of pressure chambers to evaluate the water status of plants has been widely validated in several crops, including grapevines (Choné *et al*., 2001; Yuste *et al*., 2004). However, the destructive context of the method is a limiting factor for the frequency of measurements, especially on specific small-scale assays using potted plants. Considering that one leaf must be excised on every data collection point and the vines tested in this work were no bigger than 15 nodes, the decision of when to perform the analysis became challenging (Rodriguez-Dominguez *et al*., 2022). The excision of leaves also reflects on plant growth *via* photosynthesis surface availability and transpiration rate, which could generate a bias for drought assay experiments (Greer, 2012), reinforcing the necessity of the development of new, non-destructive tools that can provide precise data regarding plant water status without interfering in the plant development.

2. Water deficit consequences in grapevine photosynthetic activity and development

In the four experiments, well-known plant morphological and physiological effects of water deficit stress were observed in the tested grapevines. Photosynthetic activity was monitored in all plants during the whole experiment. From day 7, a significant reduction of net photosynthesis (*A*), given by the rate of leaf CO_2 assimilation (carboxylation) and release (photorespiration) was detected on both trials 1 and 2 (Figure 4A). Comparing WW-1 and WD-1, a reduction of 83.5 % of net photosynthesis could be seen on day 7 (7.22 ± 0.47 *vs*. 1.19 ± 0.44 µmol CO_2 $m^{-2}s^{-1}$) and no more activity was detected on day 14 (Figure 4A). Similar results were found between WW-2 and WD-2, with a reduction of 88.7 % of the *A* index in the same period (day 7: 4.78 ± 0.36 *vs*. 0.54 ± 0.20 µmol CO_2 $m^{-2}s^{-1}$). From day 10 no more photosynthetic activity was detected on WD-2 treatment (Figure 4A). The same was found when stomata conductance was measured. Stomatal conductance (*gs*) is the diffusion of CO_2, H_2O vapour, and O_2, through the plant stomata, functioning as a reference of stomatal opening in response to

environmental conditions (Damour *et al*., 2010). Decreasing in *gs* level represents an increase in leaf water deficit. As expected, and seen for net photosynthesis, day 7 revealed a significant reduction of *gs* on WD-1 and WD-2 compared to well-watered plants (12.12 ± 2.96 and 10.62 ± 2.31 *vs*. 106.75 ± 10.05 and 60.1 ± 6.30 mmol H_2O $m^{-2}s^{-1}$; Figure 4B).

After 2 days of reduced irrigation on long-moderate water deficit stress assays, we detected that the net photosynthesis activity decreased by 54.7 % on day 7 for WD-3 (Figure 4C). No significant differences were observed in the same period (day 9) for WD-4 (Figure 4C). The same was observed for stomatal conductance (Figure 4D) which could indicate that a shorter acclimatation period led to a faster plant photosynthetic activity response to hydric deficit. As already mentioned, WD-3 presented a lower number of leaves compared to WD-4, which could also explain the faster decrease in net photosynthesis and *gs*. At the end of both assays, no more leaf photosynthesis or *gs* activity could be detected (Figure 4C and 4D).

Interestingly, a reduction of both *A* and *gs* index in plants not submitted to water deficit was observed in all tested trials. The fact could be explained by a climate-chamber effected. Natural light offers a rich spectral distribution across various wavelengths, which provides a more advantageous environment for growth than fluorescent lighting conditions (Jung and Arar, 2023), improving photosynthesis performance.

Besides net photosynthesis and stomatal conductance, the transpiration, vapour pressure deficit (VPD), water use efficiency (WUE), and sub-stomatal CO_2 concentration (Ci) were evaluated in all tested vines (Figures S2, S3 and S4). As expected, after one week of water privation, WD1 and WD2 plants showed a significant decrease in leaf transpiration and WUE compared to WW1-2. In agreement, VPD and Ci increased in the same period (Figure S2). The same was observed for trial 4 during water deficit periods (Figure S3). In trial 3 no clear differences between treatments could be detected (Figure S4).

Reduction of photosynthetic activity due to water stress has been already reported in different cultivars of grapevines (Flexas *et al*., 2002; Gambetta *et al*., 2020). In field trials conducted by Gómez-del-Campo *et al*. (2002), the photosynthesis rate was reduced by 44 and 48 % for Chardonnay and Airén cultivars in response to water stress. In agreement, the climate-chamber assays performed in this work using Cabernet-Sauvignon resulted in similar reductions even though they were exposed to controlled conditions (Figure 4).

To evaluate plant development under water stress, grapevines were assessed weekly regarding length, stem diameter and number of nodes. The growth of vines was reported using the absolute growth rate (AGR), indicating the amount of stem length increment (mm) per day. On short-severe trials 1 and 2, a reduction of AGR could be observed after 7 days (Figure 5A). On day 7, WD-2 AGR decreased twofold compared to WW-2 (3.82 ± 0.70 *vs*. 1.86 ± 0.38 mm.day^{-1}). For long-moderate assays 3 and 4, the reduction AGR was

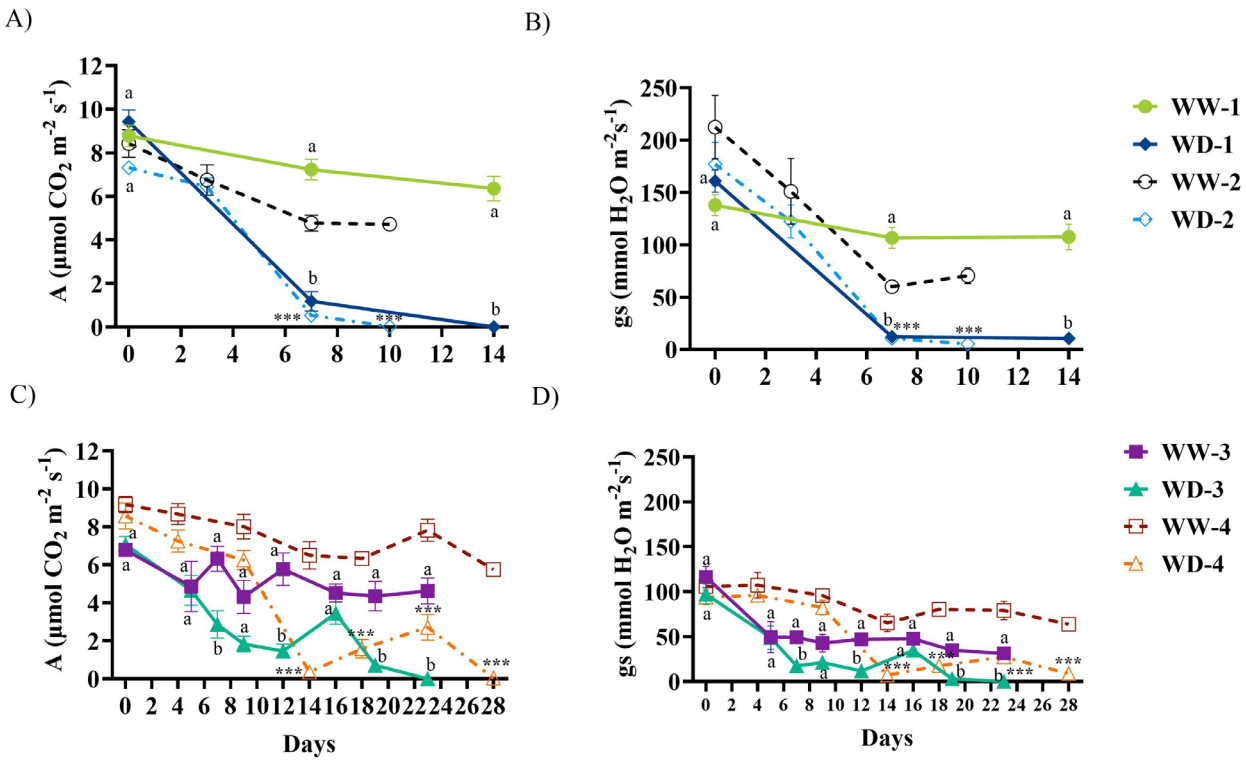


FIGURE 4. Net photosynthesis and stomatal conductance of grapevines under drought stress.

The leaf net photosynthesis (*A*) and stomatal conductance (*gs*) were measured using a portable photosynthesis system in all plants from trials 1 and 2 (A and B) and 3 and 4 (C and D). Abbreviations and statistic representations are the same as demonstrated in Figure 3.

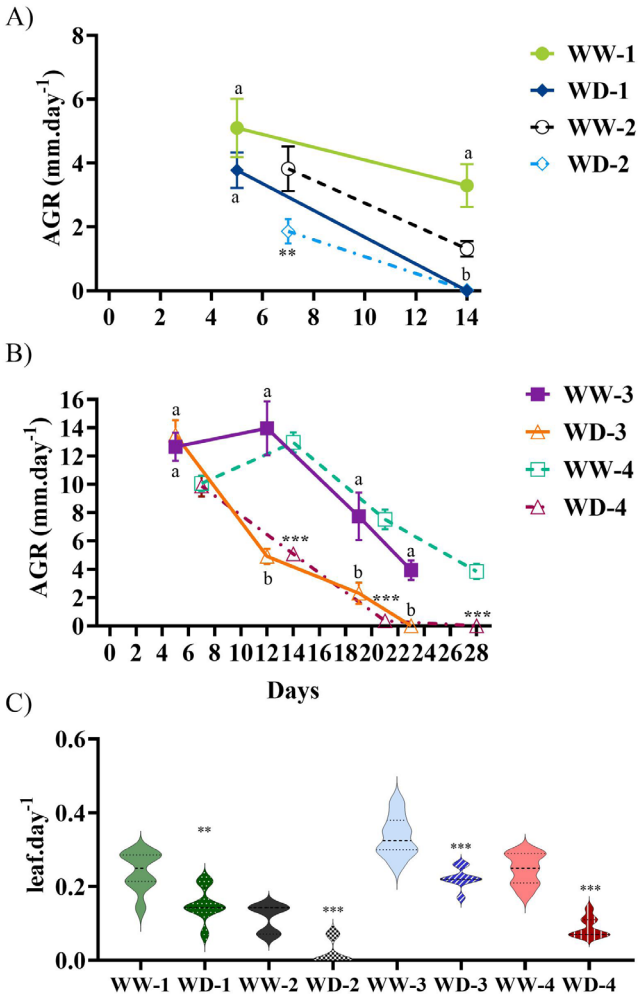


FIGURE 5. Grapevines development under water deficit stress.

Absolute growth rate (AGR) was determined every week for all tested plants from trials 1 and 2 (A) and 3 and 4 (B) based on stem growth. The number of nodes of each plant was also counted every week to estimate leaf emergence rate (C). The same letters represent a lack of statistically significant differences between treatments in the same trial for trials 1 and 3. Asterisks were used for the leaf emergence rate plot and when AGR of trials 2 and 4 were evaluated (***—$p < 0.05$). Values are represented as mean ± SEM.

observed a few days later, as expected (Figure 5B). On day 12, WD-3 AGR was reduced 2.8 times in comparison to WW-3 (13.97 ± 1.91 *vs*. 4.91 ± 0.53 mm.day^{-1}). Accordingly, a 2.5 reduction in AGR could be observed on WD-4 compared to the control group WW-4 (day 14: 12.96 ± 0.71 *vs*. 5.01 ± 0.45 mm.day^{-1}). As observed for photosynthetic activity, a negative climate-chamber effect could also be found for AGR. No more plant growth was detected on any WD-1, WD-2, WD-3 and WD-4 grapevines at the end of the experiments (Figure 5A and 5B). Leaf emergence rate (LER) was also affected by water deficit stress. Independently of the water deficit stress experiment (short-severe or long-moderate), a significant decrease of LER was observed on WD plants compared to WW (Figure 5C). The thickness of the stem diameter of WD vines was lower compared to control, especially when plants reached severe water stress (Figure S5).

Another well-known effect of water deficit is the reduction of plant biomass accumulation (Seleiman *et al*., 2021). To evaluate if any specific part of the plant would be more affected than others, we split the vines into leaves, stems, and roots to assess biomass separately. The results show generally a reduced overall biomass in water-stressed plants, regardless of the trial or plant organ (Figure S6A). These results were confirmed by biomass allocation, where no differences were observed between leaves, stems and roots (Figure S6B). Interestingly, differences in the S/R ratio of the WD group compared to WW could only be observed in long-moderate trials 3 and 4 (Figure S6B) where a significant reduction was observed under water deficit stress. Even if drought increases root mortality, the drought-induced decrease in root biomass is still lower than in shoot biomass, leading to a lower S/R (Kou *et al*., 2022; Zhou *et al*., 2018). Moreover, experiments with potted cv. Merlot vines demonstrated that drought conditions caused a drastic reduction of shoot elongation and total plant leaf area development in favour of greater biomass allocation and partitioning towards roots (Vuerich *et al*., 2021). The fact that we could not see the same differences in S/R on trials 1 and 2 can putatively be attributed to the severity and velocity of assays 1 and 2.

Regarding plant water content, leaves were the plant organ where more accentuated reductions were observed for all tested trials (Figure S6C). Around 90 % of leaf water loss was estimated for WD-1, WD-2 and WD-4 while this value drops to 70 % for WD-3 (Figure S6C). Additionally, WD-plants from long-moderate trials 3 and 4 presented an increased residual water content compared to short-severe trials 1 and 2 (WD-1: 4.64 ± 0.744; WD-2: 3.42 ± 0.51; WD-3: 8.23 ± 0.82; WD-4: 8.81 ± 1.11 g$H_2$0.plant^{-1}; Figure S6C).

3. The use of electrophysiology to infer water status on grapevines

Datasets from electrical potential recordings of trials 1-3 in both WW and WD groups were used to develop two distinct grapevine drought stress prediction models: a binary classifier (predicting the drought status of a plant) and a regression model (predicting Ψpd). The binary classifier approach is simpler and easier to train, but its output, expressed in relative probability units, may not be widely used in vine research or by grapevine growers. In contrast, the regression model requires more precise data labelling and a more advanced modelling approach, but its output is a predicted Ψpd in MPa, which is more intuitively understood by a broad audience of vine researchers, plant physiologists, and agronomists. The discrimination capabilities and precision of both models were compared by evaluating their performance on the two test sets.

3.1. Classification model

The binary classification model results show that the model can differentiate between WW and WD data used during the training phase on the train set (Figure 6A), as well as on the set T123 (Figure 6B). As explained in the methods

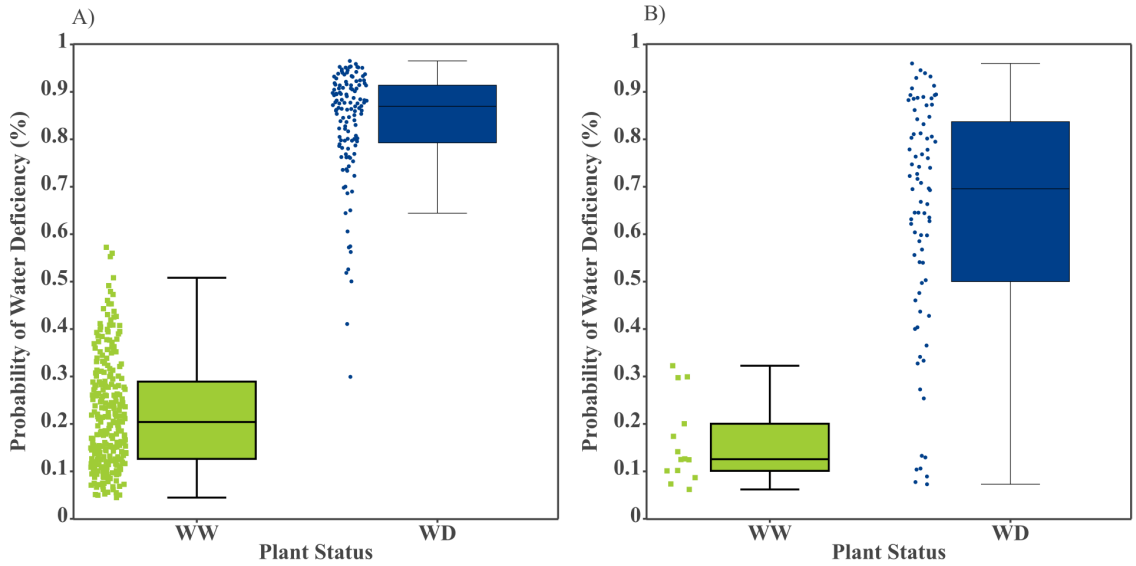


FIGURE 6. Classification model predictions on the train set and first test set (T123).

(A) The Classifier's predictions of plant water status on the train set consisted of the data used by the model during training to learn to differentiate between both states set as a function of plant status. (B) The Classifier's predictions of plant water status on the test set consisted of an unseen set of plants from the same experiments as the train set, used to validate the model's performance after training. WW-well watered, WD-water deficit. Dots represent classification probability values of individual data windows. Box plots indicate the median, interquartile range and minimal and maximal data values excluding outliers.

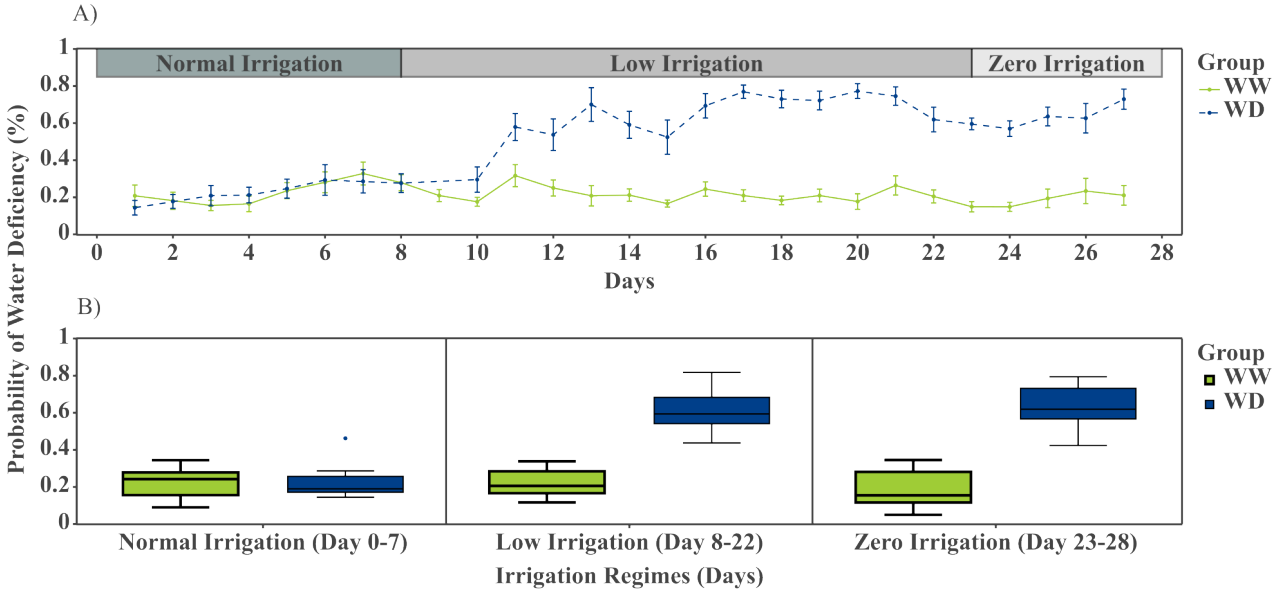


FIGURE 7. Classification model predictions on unseen data from the fourth trial (T4).

(A) Time courses of mean predictions of the water deficiency per group for T4. The three irrigation periods are labelled at the top of the plot. (B) Quantitative comparison of classifier's predictions on T4 as a function of plant status, in periods of different irrigation regimes. WW-well watered, WD -water deficit. Box plots indicate the median, interquartile range and minimal and maximal data values excluding outliers.

section, T123 consists of a subset of plants from the first 3 experiments that are not seen by the model during training. The results here demonstrate the ability of the model to predict water deficiency in plants in the same experiments as the ones used in training.

However, to test the generalisation capabilities of the model, we reserved the fourth experiment to create the test set T4. Both groups are predicted as having a low probability of water deficiency during the normal irrigation period (days 1-8), with the probability increasing to over 0.5 for the WD group after three days into the low irrigation period (days 9-11; Figure 7A). From there, the probability stays high for the WD group, while it remains low throughout the trial for the WW group (days 12-27). A quantitative comparison of the groups across irrigation periods demonstrates the model's successful differentiation between the two watering states (Figure 7B).

These results show that our binary classification model is successful in differentiating between WW and WD plants based on features extracted from the plants' electrical potential recordings. Acknowledging that such a classifier

outputting relative probabilities of water deficiency may lack practical usefulness for researchers and especially growers, a regression model attempting to directly predict the Ψpd of the vines from their electrical potential recordings was developed.

3.2. Regression model

Correlation analysis between the measured Ψpd and the predicted Ψpd for the training data set shows a strong correlation, with a linear fit yielding an R^2 score of 0.98, indicating that the model has effectively learned the underlying patterns and achieved high accuracy (Figure 8A). However, the correlation plot for the T123 test set reveals a weaker performance (Figure 8B). The linear fit on this test set produces an R^2 score of 0.23. Analysis of the slope of the linear fit suggests that the model tends to better predict higher than lower Ψpd, which reflects in a more accurate detection of water deficit in early stages (Figure 8B).

Accordingly, regression analysis of unseen experiment T4 (measured Ψpd values, excluding the interpolated feature vectors), yields an R^2 score of 0.16, indicating a poor fit, similar to the results seen with T123. However, the linear fit improves to 0.35 in the Ψpd range between –1.5 and 0 MPa (Figure 9A). This indicates that although the regression model may not be entirely accurate, it is more effective in detecting early shifts in plant water status. This capability offers valuable opportunities for proactive vineyard management, helping to prevent the more severe consequences of water deficit on plant growth and development (Charrier *et al*., 2018; Gambetta *et al*., 2020).

While examining individual predictions and the direct correlation between measured and predicted Ψpd provides a detailed assessment of the model's performance, practical applications would more likely involve predicting water deficiency trends across groups of vines rather than on individual plants. Using this aggregation approach, the test predictions indicate that the regression model can effectively differentiate between WW and WD conditions on unseen data (Figure 9B). The model shows that both groups exhibit a low probability of water deficiency during the normal irrigation period. However, once the low irrigation regime begins, the probability rapidly increases for the WD group (8-15 days). This distinction between the groups remains consistent during the later stages of the low irrigation period, with a slight decrease observed in the extreme, zero irrigation period.

3.3. Comparing both modelling approaches

Both model precision was evaluated based on different approaches. For the classification model, the evaluation of T123 predictions yielded a precision score of 1.0 and a recall score of 0.42. The regression model aimed to predict the value of Ψpd rather than the status of the plant (WW or WD). Unlike the classification model, precision and recall scores are not applicable for regression tasks. To facilitate comparison with the classification model, we defined the threshold as a Ψpd lower than –0.9 MPa, which represents the transitions from moderate to severe water stress (van Leeuwen *et al*., 2009; Lovisolo *et al*., 2010; Rienth and Scholasch, 2019). Subsequently, we constructed a confusion matrix for the regression model (Table S1) based on its predictions on T123 and computed precision and recall scores of 0.46 and

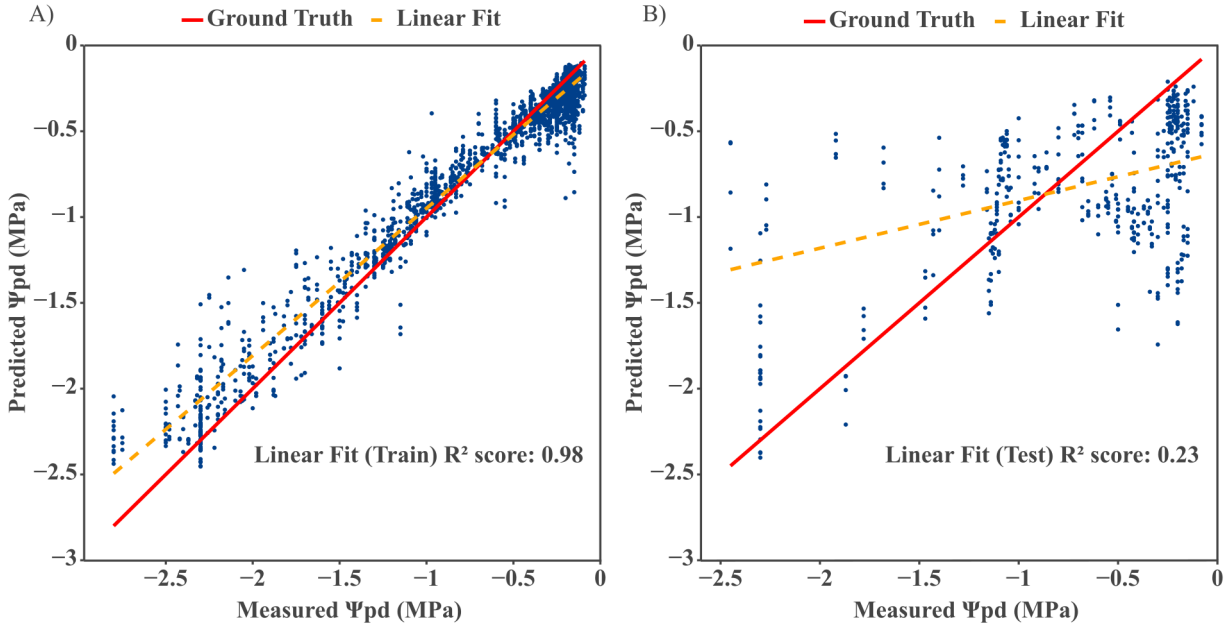


FIGURE 8. Regression analysis of measured and model-predicted water potential values obtained from the train and first test set (T123).

(A) Correlation between the measured Ψpd and the regression model's predicting Ψpd on the train set. (B) Predictions on test set T123. Multiple feature vectors with the same label (either from the actual measurement or from the interpolation between the measurements), resulted in multiple model predictions for the same label and created vertical groups about measured Ψpd. The red line represents the ideal fit, while the orange dashed line represents the actual fit.

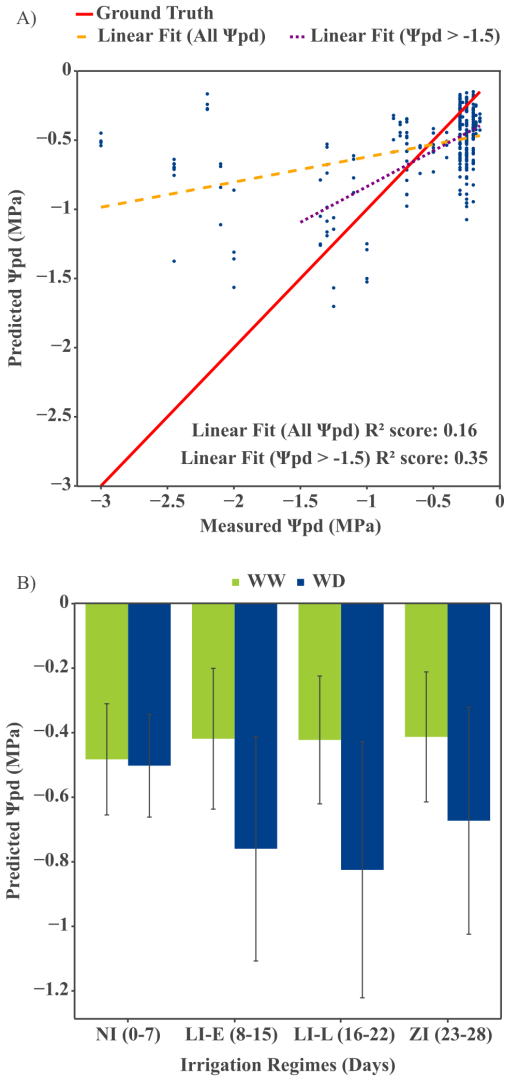


FIGURE 9. Regression model performance on unseen test set from trial 4.

(A) Dependence between measured predawn leaf water potential (Ψpd) and the regression model's predicted Ψpd. The red line represents the ground truth, while the orange dashed line represents the linear fit of all the data. The purple dotted line is a linear fit of the data with measured Ψpd > −1.5. (B) Quantitative comparison of the well-watered (WW) and water deficit subjected (WD) groups of plants in normal (NI), low (LI) and zero (ZI) irrigation regime periods. LI is split into early (LI-E) and late (LI-L) periods for finer-scale analysis. Bar charts represent the mean predicted Ψpd per group ± SD.

0.55, respectively. This approach allows for a standardised comparison between the classification and regression models.

Both models have low precision-recall average scores. However, it is important to note that these metrics focus on individual windows. In practical applications, the drought status of a field is determined by aggregating data from multiple windows originating from various plants, thereby mitigating inter-plant variability, as discussed above and illustrated in Figure 9B.

In summary, while the classification model is capable of correctly classifying plants into WW or WD states based on features computed on electrophysiological data over 24-hour windows, the regression model struggles to generalise past the training data. The classification approach shows good classifying potential on both unseen plants (T123) and unseen experiments (T4). In contrast, the regression model, which aims to directly predict the Ψpd of a plant, does not appropriately generalise to unseen plants (T123) or unseen experiments (T4). This result is unsurprising at this early stage of development since regression models are known to be more data-hungry compared to their classification model counterparts (Bishop and Nasrabadi, 2006; Guyon and Elisseeff, 2003). In regression, the model attempts to predict a continuous value, which requires capturing the underlying patterns and variations in the data in a more 'fine-grained' way. On the other hand, classification problems involve predicting discrete labels (in our case WW or WD), which here seems to be achievable with less data. Furthermore, the distribution of Ψpd measurements is skewed towards higher Ψpd values, meaning we have an unbalanced dataset (Figure S7). Most of the labelled data is concentrated between –0.5 and 0 MPa and the number of samples severely decreases past –1.5 MPa. This results in the model being exposed to more examples of WW feature vectors, which may partially explain the lower variance in T123 predictions in higher Ψpd values compared to lower ones (Figure 8B)–there are too few samples to predict in T4 to support or challenge this claim. Additionally, we observe here the regression towards the mean phenomenon, where extreme observations or predictions tend to move closer to the average in subsequent observations or predictions due to their rarity. This is visible in the linear fit lines tending towards the average prediction in Figures 8B and 9A. Due to the usefulness of a model capable of automatically predicting Ψpd on vine plants based on electrophysiological data, we believe the regression approach should be further pursued in subsequent work. This would require more experiments to be conducted to increase the size of our datasets.

4. Understanding the models' decision making

In this section we use explainable artificial intelligence (AI) techniques to elucidate the opaque nature of ML models (Došilović *et al.*, 2018). Specifically, we use the Python library SHAP [SHapley Additive exPlanations; Lundberg & Lee (2017)] to quantify, using SHAP values, the contribution of each feature to the predictions of the model. SHAP values offer a detailed breakdown of the impact each feature has on the prediction: a positive SHAP value indicates that the feature contributes positively to the prediction, whereas a negative SHAP value signifies a negative contribution. The absolute magnitude of the SHAP value reflects the strength of the influence of the feature on the prediction.

Figure 10 shows the SHAP summary plot for the classification model. In the figure, each point represents a SHAP value for a feature corresponding to a single observation in the dataset. The position of the point on the x-axis indicates the direction and the magnitude of the impact on the predictions. Features are ordered by their importance, with the most

impactful features listed at the top and the colour of each point indicating the value of the feature.

The results indicate that the most impactful features were all computed from the lowest decomposition levels of the discrete wavelet decomposition (feature names ending with wavelet 9, 12 and 14). Specifically, the feature name ending with:

- (Wavelet 9) was computed from the band-pass version of the signal, covering a frequency range of $7.81 \cdot 10^{-3}$ to $1.56 \cdot 10^{-2}$ Hz;
- (Wavelet 12) was computed from the band-pass version of the signal, covering a frequency range of $6.25 \cdot 10^{-2}$ to 0.125 Hz;
- (Wavelet 14) was computed from the high-pass version of the signal, covering a frequency range of 0.25 to 0.50 Hz.

In summary, all important features were computed on band- or high-passed versions of the signal in the frequency range $[7.81 \cdot 10^{-3}, 0.50]$ Hz, indicating that these high-frequency components of the signal are particularly significant in the decision process of the model.

Figure 10 provides further insights into the important characteristics of the signal. By examining the specific features computed on the wavelet decomposition levels described above, we can understand which aspects of the signal are critical for the model:

Entropy Pairs transforms each value in the time series into one of three symbols ('A', 'B', or 'C') using an equi-probable binning method. In this method, the lowest third of the values are assigned 'A', the middle third 'B', and the highest third 'C'. Next, it evaluates the probabilities of all possible two-letter sequences ('AA', 'AB', 'BB', etc.) and calculates the entropy of these probabilities. Time series with predictable two-letter sequences (where some sequences are much more likely than others) will have low entropy values, while those with less predictable sequences (where all sequences are roughly equally likely) will have high entropy values. In the figure, two clear clusters of values are noticeable, represented by different colours. Low values, shown in blue, decrease the final output of the model, while high values, indicating increased randomness, significantly impact the model output by increasing the predicted probability of water deficiency.

IQR measures the statistical dispersion or spread of the data points in the signal window. The IQR is calculated as the difference between the 75th percentile (Q3) and the 25th percentile (Q1) of the data. This metric captures the range within which the central 50 % of the values lie, effectively summarizing the variability in the middle portion of the data set. A high IQR indicates that the data points are widely spread around the median, suggesting high variability or volatility. Conversely, a low IQR suggests that the data points are closely clustered around the median, indicating low variability or more stability. In the figure, two distinct regimes can be observed. Large values, depicted in red and indicating a larger variability in the data, increase the predicted probability of water deficiency, while low values, shown in blue, negatively influence the model's output.

Low Freq Power calculates the relative power in the lowest 20 % of frequencies. It assigns high values to time series with significant power in low frequencies and low values to those with most of their power concentrated in higher frequencies. The area under the power spectrum is estimated in linear space, using Welch's method with a rectangular window to estimate the power spectral density. In Figure 10, two distinct regimes are evident for this feature: low power in low frequencies tends to decrease the model output, while high power in low frequencies decreases the model output.

These three top features corroborate the hypothesis that plants in a WD state exhibit higher activity or noise in high frequencies, as opposed to plants in a WW state. Understanding this relationship could fully unlock the potential of plant electrophysiology for monitoring plant water status. However, the multitude of physiological processes affected by drought stress, which are potentially linked in parallel with the displacement of charged molecules, makes it challenging to identify the primary process most reflected in the ML model features.

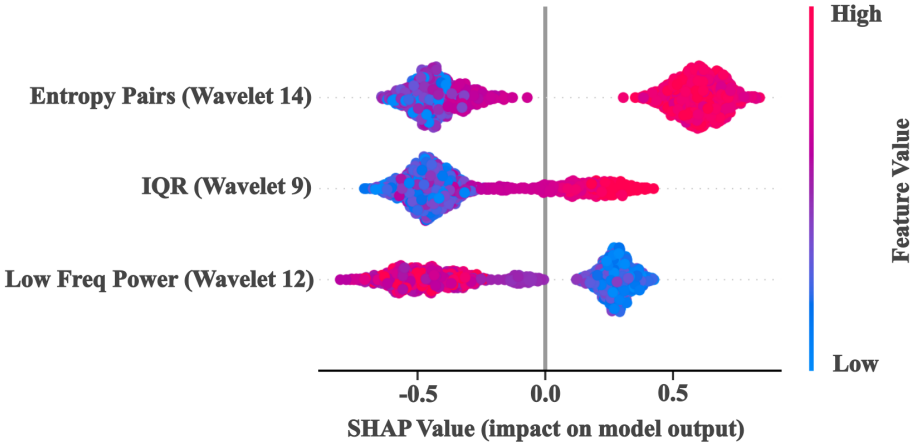


FIGURE 10. Feature importance for the classification model.

SHAP summary plot for the classification model describing the 3 most influential features in the model's decision-making. Red dots indicate a high feature value, while blue dots indicate a low feature value.

CONCLUSION

In conclusion, the application of electrophysiology for modelling water status in grapevines has yielded promising results through the development of two distinct prediction models for drought stress. The classification model demonstrated robust performance in distinguishing between WW and WD conditions across both T123, which consists of unseen plants from trials seen during training and a completely unseen experiment (T4). Meanwhile, although the regression model aimed at predicting Ψpd values failed at generalising to unseen plants (T123) or unseen experiments (T4), it nonetheless showed encouraging results when the predictions were averaged across groups of plants. This aggregation more closely resembles the practical setting that this type of model may be used in the future to aid researchers and growers in monitoring water deficiency in vines.

The importance of key features measuring the variance or noise at high frequencies of the electrophysiological signals highlighted significant differences between WW and WD conditions. Notably, higher values in entropy pairs and IQR, as well as decreased low-frequency power at specific frequency ranges, correlated with higher probabilities of water deficiency, illustrating their utility in detecting stress responses in plants. These findings underscore the potential of electrophysiological monitoring in precision agriculture, though further research is warranted to deepen our understanding of the underlying physiological mechanisms driving these signals.

In future studies, expanding the data size and collecting data from different growing conditions where vines are exposed to various kinds of abiotic but also biotic stress to adjust and refine the models could enhance their predictive power and will ultimately support more effective management strategies for optimizing grapevine health and yield under varying water availability scenarios.

ACKNOWLEDGEMENTS

The project has received funding as part of the AGRARSENSE project from the Chips Joint Undertaking (JU) under Grant Agreement N° 101095835 and is supported by the Swiss Confederation (State Secretariat for Education Research and Innovation SERI and the Federal Office for Agriculture FOAG) and the Chips Joint Undertaking and its members, including top-up funding by national funding authorities of Sweden, Czechia, Finland, Ireland, Italy, Latvia, Netherlands, Norway, Poland, and Spain. The post-doc of Esteban Alfonso was partly founded by the Swiss National Science Fondation (Grant number IZCOC0_189896). We also would like to thank Arnaud Pernet for technical support regarding the climate chambers.

REFERENCES

Akiba, T., Sano, S., Yanase, T., Ohta, T., & Koyama, M. (2019). *Optuna: A Next-generation Hyperparameter Optimization Framework*. https://github.com/pfnet/optuna/

Amin, H. U., Malik, A. S., Ahmad, R. F., Badruddin, N., Kamel, N., Hussain, M., & Chooi, W. T. (2015). Feature extraction and classification for EEG signals using wavelet transform and machine learning techniques. *Australasian Physical & Engineering Sciences in Medicine*, *38*(1), 139–149. https://doi.org/10.1007/S13246-015-0333-X

Araújo, S. O., Peres, R. S., Ramalho, J. C., Lidon, F., & Barata, J. (2023). Machine Learning Applications in Agriculture: Current Trends, Challenges, and Future Perspectives. *Agronomy 2023, Vol. 13, Page 2976*, *13*(12), 2976. https://doi.org/10.3390/AGRONOMY13122976

Bishop, C.M. and Nasrabadi, N.M. (2006). Pattern Recognition and Machine Learning. *4*(4), Springer, New York, 738.

Charrier, G., Delzon, S., Domec, J. C., Zhang, L., Delmas, C. E. L., Merlin, I., Corso, D., King, A., Ojeda, H., Ollat, N., Prieto, J. A., Scholach, T., Skinner, P., van Leeuwen, C., & Gambetta, G. A. (2018). Drought will not leave your glass empty: Low risk of hydraulic failure revealed by long-term drought observations in world's top wine regions. *Science Advances*, *4*(1). https://doi.org/10.1126/SCIADV.AAO6969

Chen, T., & Guestrin, C. (2016). XGBoost: A scalable tree boosting system. *Proceedings of the ACM SIGKDD International Conference on Knowledge Discovery and Data Mining*, *13-17-August-2016*, 785–794. https://doi.org/10.1145/2939672.2939785

Choné, X., van Leeuwen, C., Dubourdieu, D., & Gaudillère, J.P. (2001). Stem Water Potential is a Sensitive Indicator of Grapevine Water Status. *Annals of Botany*, *87*(4), 477–483. https://doi.org/10.1006/ANBO.2000.1361

Damour, G., Simonneau, T., Cochard, H., & Urban, L. (2010). An overview of models of stomatal conductance at the leaf level. *Plant, Cell & Environment*, *33*(9), 1419–1438. https://doi.org/10.1111/J.1365-3040.2010.02181.X

Došilović, F. K., Brcic, M., & Hlupic, N. (2018). Explainable artificial intelligence: A survey. *2018 41st International Convention on Information and Communication Technology, Electronics and Microelectronics, MIPRO 2018 - Proceedings*, 210–215. https://doi.org/10.23919/MIPRO.2018.8400040

Fawaz, H. I., Forestier, G., Weber, J., Idoumghar, L., & Muller, P.-A. (2018). Deep learning for time series classification: a review. *Data Mining and Knowledge Discovery*, *33*(4), 917–963. https://doi.org/10.1007/s10618-019-00619-1

Feng, W., Lindner, H., Robbins, N. E., & Dinneny, J. R. (2016). Growing Out of Stress: The Role of Cell- and Organ-Scale Growth Control in Plant Water-Stress Responses. *The Plant Cell*, *28*(8), 1769. https://doi.org/10.1105/TPC.16.00182

Flexas, J., Bota, J., Escalona, J. M., Sampol, B., & Medrano, H. (2002). Effects of drought on photosynthesis in grapevines under field conditions: An evaluation of stomatal and mesophyll limitations. *Functional Plant Biology*, *29*(4), 461–471. https://doi.org/10.1071/PP01119

Fromm, J., & Lautner, S. (2007). Electrical signals and their physiological significance in plants. *Plant, Cell & Environment*, *30*(3), 249–257. https://doi.org/10.1111/J.1365-3040.2006.01614.X

Gambetta, G. A., Herrera, J. C., Dayer, S., Feng, Q., Hochberg, U., & Castellarin, S. D. (2020). The physiology of drought stress in grapevine: towards an integrative definition of drought tolerance. *Journal of Experimental Botany*, *71*(16), 4658–4676. https://doi.org/10.1093/JXB/ERAA245

Gil, P. M., & Vargas, A. I. (2023). Stem electrical potential variations may aid in the early detection of drought stress in fruit-bearing trees. *Int. J. Agric. Nat. Resour*, *50*(3), 116–129. https://doi.org/10.7764/ijanr.v50i3.2552

Gómez-del-Campo, M., Ruiz, C., & Lissarrague, J. R. (2002). Effect of water stress on leaf area development, photosynthesis, and productivity in Chardonnay and Airén grapevines. *American Journal of Enology and Viticulture*, *53*(2), 138–143. https://doi.org/10.5344/AJEV.2002.53.2.138

Goodfellow, I., *et al*. (2016). Deep Learning. MIT Press, Cambridge, MA. http://www.deeplearningbook.org

Greer, D. H. (2012). Modelling leaf photosynthetic and transpiration temperature-dependent responses in Vitis vinifera cv. Semillon grapevines growing in hot, irrigated vineyard conditions. *AoB PLANTS*, *2012*(1), 9. https://doi.org/10.1093/AOBPLA/PLS009

Guyon, I., & De, A. M. (2003). An Introduction to Variable and Feature Selection André Elisseeff. *Journal of Machine Learning Research*, *3*, 1157–1182.

Hastie, T., Tibshirani, R., & Friedman, J. (2009). *The Elements of Statistical Learning*. https://doi.org/10.1007/978-0-387-84858-7

Jung, C., & Arar, M. (2023). Natural vs. Artificial Light: A Study on the Influence of Light Source on Chlorophyll Content and Photosynthetic Rates on Indoor Plants. *Buildings 2023, 13, Page 1482*, *13*(6), 1482. https://doi.org/10.3390/BUILDINGS13061482

Kaufman, S., Rosset, S., Perlich, C., & Stitelman, O. (2012). Leakage in data mining. *ACM Transactions on Knowledge Discovery from Data (TKDD)*, *6*(4). https://doi.org/10.1145/2382577.2382579

Kou, X., Han, W., & Kang, J. (2022). Responses of root system architecture to water stress at multiple levels: A meta-analysis of trials under controlled conditions. *Frontiers in Plant Science*, *13*, 1085409. https://doi.org/10.3389/FPLS.2022.1085409/BIBTEX

Kurenda, A., Jenni, D., Lecci, S., & Buchholz, A. (2024). Bringing light into the dark—plant electrophysiological monitoring of root knot nematode infestation and real-time nematicide efficacy. *Journal of Pest Science*, 1–15. https://doi.org/10.1007/S10340-024-01798-7/METRICS

Lovisolo, C., Perrone, I., Carra, A., Ferrandino, A., Flexas B, J., Medrano, H., & Schubert, A. (2010). *Drought-induced changes in development and function of grapevine (Vitis spp.) organs and in their hydraulic and non-hydraulic interactions at the whole-plant level: a physiological and molecular update*. https://doi.org/10.1071/FP09191

Lubba, C. H., Sethi, S. S., Knaute, P., Schultz, S. R., Fulcher, B. D., & Jones, N. S. (2019). catch22: CAnonical Time-series CHaracteristics: Selected through highly coMParative time-series analysis. *Data Mining and Knowledge Discovery*, *33*(6), 1821–1852. https://doi.org/10.1007/S10618-019-00647-X/TABLES/5

Lundberg, S. M., & Lee, S. I. (2017). A Unified Approach to Interpreting Model Predictions. *Advances in Neural Information Processing Systems*, *2017-December*, 4766–4775. https://arxiv.org/abs/1705.07874v2

Mallat, S. G. (1989). A Theory for Multiresolution Signal Decomposition: The Wavelet Representation. *IEEE Transactions on Pattern Analysis and Machine Intelligence*, *11*(7), 674–693. https://doi.org/10.1109/34.192463

Najdenovska, E., Dutoit, F., Tran, D., Rochat, A., Vu, B., Mazza, M., Camps, C., Plummer, C., Wallbridge, N., & Raileanu, L. E. (2021). Identifying general stress in commercial tomatoes based on machine learning applied to plant electrophysiology. *Applied Sciences (Switzerland)*, *11*(12), 5640. https://doi.org/10.3390/APP11125640/S1

Pons, A., Allamy, L., Schüttler, A., Rauhut, D., Thibon, C., & Darriet, P. (2017). What is the expected iMPact of climate change on wine aroma compounds and their precursors in grape? *OENO One*, *51*(2), 141–146. https://doi.org/10.20870/OENO-ONE.2017.51.2.1868

Rienth, M., & Scholasch, T. (2019). State-of-the-art of tools and methods to assess vine water status. *OENO One*, *53*(4), 619–637. https://doi.org/10.20870/OENO-ONE.2019.53.4.2403

Rienth, M., Torregrosa, L., Luchaire, N., Chatbanyong, R., Lecourieux, D., Kelly, M. T., & Romieu, C. (2014). Day and night heat stress trigger different transcriptomic responses in green and ripening grapevine (*Vitis vinifera*) fruit. *BMC Plant Biology*, *14*(1), 1–18. https://doi.org/10.1186/1471-2229-14-108/FIGURES/6

Rienth, M., Vigneron, N., Darriet, P., Sweetman, C., Burbidge, C., Bonghi, C., Walker, R. P., Famiani, F., & Castellarin, S. D. (2021). Grape Berry Secondary Metabolites and Their Modulation by Abiotic Factors in a Climate Change Scenario–A Review. *Frontiers in Plant Science*, *12*, 643258. https://doi.org/10.3389/FPLS.2021.643258

Rodriguez-Dominguez, C. M., Forner, A., Martorell, S., Choat, B., Lopez, R., Peters, J. M. R., Pfautsch, S., Mayr, S., Carins-Murphy, M. R., McAdam, S. A. M., Richardson, F., Diaz-Espejo, A., Hernandez-Santana, V., Menezes-Silva, P. E., Torres-Ruiz, J. M., Batz, T. A., & Sack, L. (2022). Leaf water potential measurements using the pressure chamber: Synthetic testing of assumptions towards best practices for precision and accuracy. *Plant, Cell & Environment*, *45*(7), 2037–2061. https://doi.org/10.1111/PCE.14330

Roelfsema, M. R. G., Levchenko, V., & Hedrich, R. (2004). ABA depolarizes guard cells in intact plants, through a transient activation of R- and S-type anion channels. *The Plant Journal : For Cell and Molecular Biology*, *37*(4), 578–588. https://doi.org/10.1111/J.1365-313X.2003.01985.X

Scholander, P. F., Hammel, H. T., Bradstreet, E. D., & Hemmingsen, E. A. (1965). Sap Pressure in Vascular Plants: Negative hydrostatic pressure can be measured in plants. *Science (New York, N.Y.)*, *148*(3668), 339–346. https://doi.org/10.1126/SCIENCE.148.3668.339

Scholasch, T., & Rienth, M. (2019). Review of water deficit mediated changes in vine and berry physiology; Consequences for the optimization of irrigation strategies. *OENO One*, *53*(3), 423–444. https://doi.org/10.20870/OENO-ONE.2019.53.3.2407

Seleiman, M. F., Al-Suhaibani, N., Ali, N., Akmal, M., Alotaibi, M., Refay, Y., Dindaroglu, T., Abdul-Wajid, H. H., & Battaglia, M. L. (2021). Drought stress iMPacts on plants and different approaches to alleviate its adverse effects. *Plants*, *10*(2), 1–25. https://doi.org/10.3390/PLANTS10020259

Tran, D., Dutoit, F., Najdenovska, E., Wallbridge, N., Plummer, C., Mazza, M., Raileanu, L. E., & Camps, C. (2019). Electrophysiological assessment of plant status outside a Faraday cage using supervised machine learning. *Scientific Reports 2019 9:1*, *9*(1), 1–9. https://doi.org/10.1038/s41598-019-53675-4

van Leeuwen, C., Destrac-Irvine, A., Dubernet, M., Duchêne, E., Gowdy, M., Marguerit, E., Pieri, P., Parker, A., De Rességuier, L., & Ollat, N. (2019). An update on the iMPact of climate change in viticulture and potential adaptations. *Agronomy*, *9*(9). https://doi.org/10.3390/AGRONOMY9090514

van Leeuwen, C., Tregoat, O., Choné, X., Bois, B., Pernet, D., & Gaudillére, J. P. (2009). Vine water status is a key factor in grape ripening and vintage quality for red Bordeaux wine. How can it be assessed for vineyard management purposes? *OENO One*, *43*(3), 121–134. https://doi.org/10.20870/OENO-ONE.2009.43.3.798

van Leeuwen, C., Sgubin, G., Bois, B., Ollat, N., Swingedouw, D., Zito, S., & Gambetta, G. A. (2024). Climate change iMPacts and adaptations of wine production. *Nature Reviews Earth & Environment 2024 5:4*, *5*(4), 258–275. https://doi.org/10.1038/s43017-024-00521-5

Vilagrosa, A. A., Chirino, E. E., J-J Peguero-Pina, J.-J., Severien S Barigah, T. T., Cochard, H. H., & Gil-Pelegrin, E. E. (2012). Xylem cavitation and embolism in plants living in water-limited ecosystems. *Plant responses to drought stress, Springer, 466*. https://doi.org/10.1007/978-3-642

Vuerich, M., Braidotti, R., Sivilotti, P., Alberti, G., Casolo, V., Braidot, E., Boscutti, F., Calderan, A., Petrussa, E., & Finkbeiner, M. (2021). *Response of Merlot Grapevine to Drought Is Associated to Adjustments of Growth and Nonstructural Carbohydrates Allocation in above and Underground Organs*. https://doi.org/10.3390/w13172336

Wang, J., Wang, Z., Li, J., & Wu, J. (2018). Multilevel Wavelet Decomposition Network for Interpretable Time Series Analysis. *Proceedings of the ACM SIGKDD International Conference on Knowledge Discovery and Data Mining*, 2437–2446. https://doi.org/10.1145/3219819.3220060

Xing, D., Chen, X., Wu, Y., Xu, X., Chen, Q., Li, L., & Zhang, C. (2019). Rapid prediction of the re-watering time point of Orychophragmus violaceus L. based on the online monitoring of electrophysiological indexes. *Scientia Horticulturae*, *256*, 108642. https://doi.org/10.1016/J.SCIENTA.2019.108642

Yuste, J., Gutierrez, I., Rubio, J. A., & Alburquerque, M. V. (2004). Leaf and stem water potential as vine water status indicators, in Tempranillo grapevine, under different water regimes in the Duero valley. *OENO One*, *38*(1), 21–26. https://doi.org/10.20870/OENO-ONE.2004.38.1.940

Zhang, C., Wu, Y., Su, Y., Xing, D., Dai, Y., Wu, Y., & Fang, L. (2020). A Plant's Electrical Parameters Indicate Its Physiological State: A Study of Intracellular Water Metabolism. *Plants*, *9*(10), 1–16. https://doi.org/10.3390/PLANTS9101256

Zhou, G., Zhou, X., Nie, Y., Bai, S. H., Zhou, L., Shao, J., Cheng, W., Wang, J., Hu, F., & Fu, Y. (2018). Drought-induced changes in root biomass largely result from altered root morphological traits: Evidence from a synthesis of global field trials. *Plant, Cell & Environment*, *41*(11), 2589–2599. https://doi.org/10.1111/PCE.13356